Computational and Theoretical Chemistry 977 (2011) 148–156

Contents lists available at SciVerse ScienceDirect

Computational and Theoretical Chemistry

journal homepage: www.elsevier.com/locate/comptc

Density functional theory study of dipicolinic acid isomers and crystalline polytypes

Richard D. Massaro, Estela Blaisten-Barojas *

Computational Materials Science Center and School of Physics, Astronomy, & Computational Sciences, George Mason University, 4400 University Dr. MS 6A2, Fairfax, VA 22030, USA

ARTICLE INFO

Article history:
Received 20 April 2011
Received in revised form 17 September 2011
Accepted 19 September 2011
Available online 29 September 2011

Keywords:
Dipicolinic acid
DPA crystal
Density functional theory
Vibrational spectrum
DPA isomers

ABSTRACT

Six isomers of dipicolinic acid (DPA) in the gas phase are predicted based on a detailed density functional theory study. Energetics include the binding energy, ionization potential, and electron affinity. Dipole moments, rotational constants, atomic charges, and Fukui functions are also calculated. Several isomerization reactions are shown as possible, with calculated reaction path and transition barriers in the range 6–14 kcal/mol. Prediction of five DPA dimers and three crystalline DPA polytypes are also reported. Vibrational analysis for monomers and dimers is calculated and compared to existing experimental results. The electronic band structure of three crystalline polytypes shows that DPA crystals are insulators. The three stable polytypes display distinct hydrogen-bonding formations that originate sheets of DPA molecules that are further stacked to form layered crystals that are energetically nearly degenerate.

1. Introduction

Powell [1,2] was the first to discover the fact that dipicolinic acid (DPA, 2,6-pyridinedicarboxylic acid), $C_5H_3N(COOH)_2$, is excreted by most or all species of germinating bacterial spores. DPA is a unique biomarker thought to protect bacterial spores because of its ability to strongly absorb ultraviolet light [3]. DPA is well-known to be a molecule with high chelation. The Ca^{2+} chelate of DPA is a major constituent of the dormant spore core, accounting for approximately 10% of total spore dry weight [4,5]. Indeed, DPA's presence within the spore medium is primarily found as a calcium chelated form, calcium dipicolinate (CaDPA), which induces and enhances bacterial spore germination [6,7]. Up to 50% of the solids excreted by the spores and up to 15% of the total dry weight of each spore are thought to be CaDPA. Additionally, CaDPA retains the characteristic of having a strong UV absorption, as does pristine DPA. While calcium and sodium bound to DPA are more often to be found in nature, there have also been studied to design optical reporters based on lanthanide elements [8–11] and molecularly imprinted polymer surfaces [12]. DPA's structural properties make this molecule an efficient functional group in the binding of anionic moieties through hydrogen-bonding and charge pairing intermolecular forces [13].

Experiments performed on wet paste and dry crystal forms of DPA and CaDPA have shown interesting effects on their fluorescence intensities [14]. The drying of DPA crystals showed an increase in the observed fluorescence as well as a broader emission peak. UV-exposed samples exhibited dramatic increases in fluorescence [15]. It has been theorized that a photochemical reaction takes place to form new molecular species or isomers in those UV-irradiated samples [15]. Experiments have illustrated the vibrational spectra, supramolecular structure of the crystal unit cell [16], and crystallography of anhydrous DPA [17,18]. Among the crystal forming DPA molecules it has been identified that neutral or zwitterion structures may form anhydrous supramolecular structures by self-association with hydrogen bonds or by $\pi \rightarrow \pi^*$ electronic transitions of the pyridine ring [18,19].

Computational investigations of DPA and CaDPA have been relatively sparse. Early calculations with small basis sets have suggested that the CO_2 groups are oriented perpendicular to the ring plane [20]. Complete active space multi-configuration self-consistent field (MCSCF) calculations have determined ground and excited state geometries and vibrational frequencies for one isomer of gas phase DPA and its anion [21]. Density functional theory and time-dependent density functional theory studies performed on DPA and its dianion showed an acceptable agreement between the calculated IR, Raman, NMR, and photo-absorption spectra as compared with experimental values [22]. The latter study reports that the lowest excited singlet state for DPA is dipole-forbidden and the first dipole-allowed transition is the excitation to the second singlet state. This study also rules out a direct singlet–triplet excitation process. Other DFT studies have addressed functionalized DPA tailored for enhanced emission properties [23,11,24–26].

To the authors' knowledge, there is no literature reporting a computational investigation of DPA isomers along with predictions of which isomers may form supramolecular self-associated dimers and crystals which are intermolecularly bonded by pairs of

* Corresponding author. Fax: +1 703 993 9300.
E-mail address: blaisten@gmu.edu (E. Blaisten-Barojas).

2210-271X/$ - see front matter © 2011 Elsevier B.V. All rights reserved.
doi:10.1016/j.comptc.2011.09.030

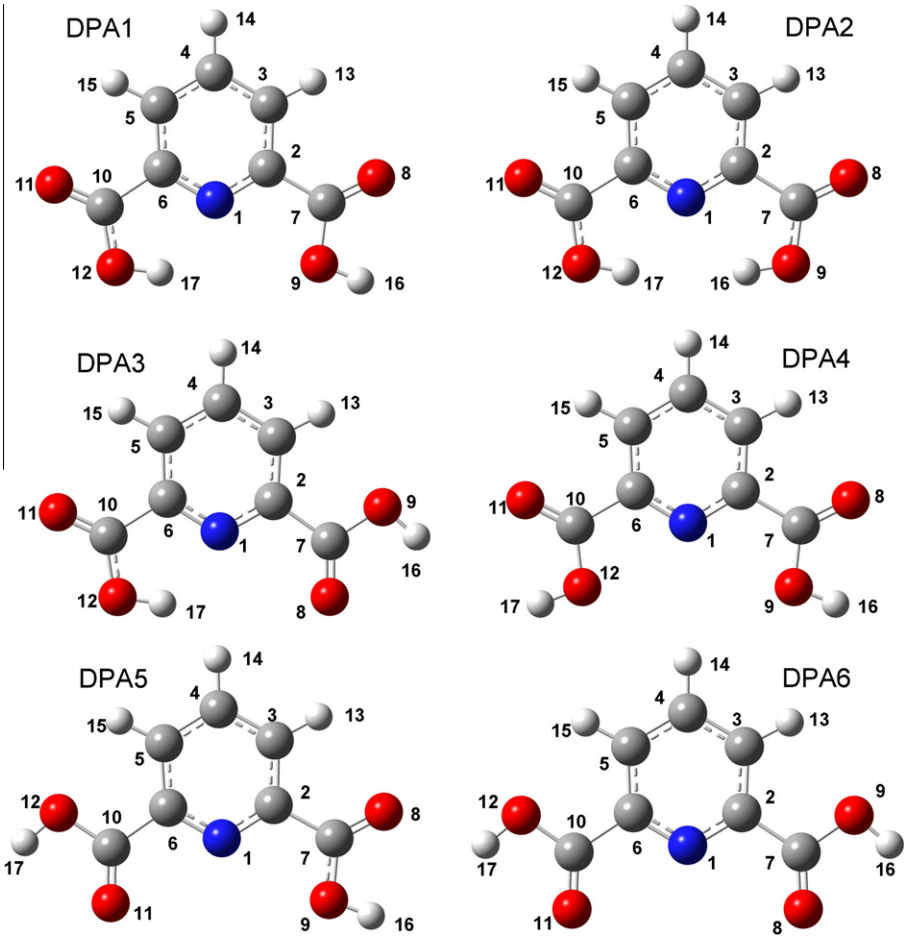

Fig. 1. Optimized structure of the six DPA isomers in the gas phase.

hydrogen bonds. In this article we put forward a thorough density functional theory (DFT) calculation to predict several stable gas phase isomers, their dimers, and crystalline polytypes. The focus is on neutral DPA structural rearrangement that excludes deprotonation. Section 2 gives an overview of the structure, energetics, vibrational analyses and isomerization pathways of six DPA isomers. Section 3 gives a description of the possible dimers that can be formed from the predicted monomers through a tandem of hydrogen bonds. Structure, energetics, and vibrational analyses are included in this section for the predicted dimers. Section 4 contains a description of three optimized crystalline polytypes of DPA, which are formed by stacking sheets of molecules arranged in parallel chains. The electronic band structure of these predicted crystals is calculated, indicating that these crystals are insulators. Concluding remarks in Section 5 close this article. Detailed structural information, IR spectra, and the vibrational spectra of the gas phase DPA isomers presented in Section 3 are provided as Supplementary data.

2. DPA isomers

All-electron density functional theory (DFT) calculations of DPA in the gas phase are performed within Becke's 3-parameter hybrid functional approach with Lee–Yang–Parr's [27] correlation functional (B3LYP) and a double-ζ basis set augmented with *d* polarization function (6-31G (d)). Structural optimizations of DPA isomers are performed with the Berny algorithm [28]. An optimized structure implies that the molecular system is in a minimum of the electronic energy. This geometry is then mechanically stable. All calculations were carried out with the Gaussian 09 package [29]. Optimized structures of the DPA predicted isomers are shown in Fig. 1. Detailed bond lengths and angles of these geometries are reported in the Supplementary data.

The electronic ground state of all of these isomers are singlets. Furthermore, it is determined that DPA isomers are also stable geometries in triplet electronic states. However, triplet states

Table 1
Singlet (S_0) and triplet (T) electronic states, electronic energies, binding energies (BE), and dipole moments of the DPA isomers. The HOMO–LUMO gap (Δ) of singlet states, electron affinities (EA), and ionization potentials (IP) are also reported. Electronic energies *E* are relative to the ^{1}DPA1 ground state energy of −17.018746 keV plus the zero point energy of 3.236 eV.

Isomer	S_0	*E* (eV)	BE (eV)	dipole (D)	EA (eV)	IP (eV)	Δ (eV)	T	*E* (eV)
DPA1	^{1}A	0	113.890	3.4, 1.8, 0	0.8	9.482	5.220	^{3}A	3.398
DPA2	^{1}A$_1$	0.046	113.843	0, 2.6, 0	0.816	9.706	5.409	^{3}A$_1$	3.50
DPA3	^{1}A	0.050	113.840	4.9, 3.9, 0	0.631	9.495	5.191	^{3}A	3.447
DPA4	^{1}A$_1$	0.144	113.746	0, 0.7, 0	0.286	9.021	5.383	^{3}A$_1$	3.392
DPA5	^{1}A	0.215	113.674	1.4, 2.9, 0	0.282	9.070	5.437	^{3}A	3.456
DPA6	^{1}A$_1$	0.296	113.594	0, 5.2, 0	0.280	9.149	5.599	^{3}A	3.652

Table 2
Atomic charges of DPA isomers calculated from the Mulliken analysis.

Atom	DPA1	DPA2	DPA3	DPA4	DPA5	DPA6
N1	−0.591	−0.663	−0.578	−0.503	−0.491	−0.479
C2	0.245	0.250	0.232	0.231	0.217	0.218
C3	−0.141	−0.140	−0.145	−0.136	−0.139	−0.138
C4	−0.107	−0.103	−0.105	−0.111	−0.109	−0.107
C5	−0.139	−0.140	−0.138	−0.136	−0.135	−0.138
C6	0.249	0.250	0.251	0.231	0.233	0.218
C7	0.560	0.589	0.562	0.555	0.559	0.560
O8	−0.462	−0.447	−0.442	−0.471	−0.437	−0.433
O9	−0.559	−0.574	−0.581	−0.548	−0.587	−0.587
C10	0.586	0.589	0.587	0.555	0.556	0.560
O11	−0.457	−0.447	−0.458	−0.471	−0.471	−0.433
O12	−0.582	−0.574	−0.581	−0.548	−0.545	−0.587
H13	0.187	0.195	0.183	0.183	0.179	0.179
H14	0.167	0.173	0.166	0.160	0.159	0.158
H15	0.190	0.195	0.190	0.183	0.183	0.179
H16	0.419	0.424	0.420	0.414	0.416	0.416
H17	0.437	0.424	0.440	0.414	0.414	0.416

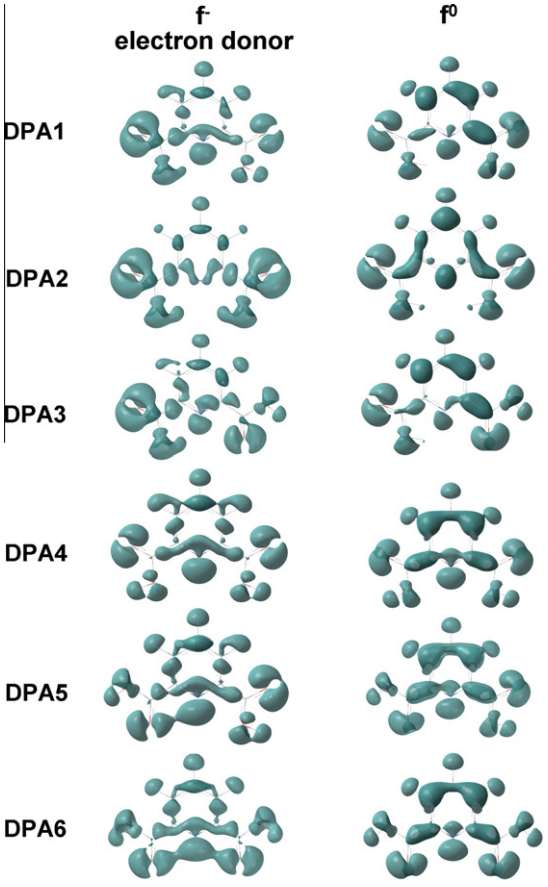

Fig. 2. Fukui functions; f^- (electron donor) and f^0 (radical attack) of DPA isomers. A value of 0.002 was used to create the positive iso-surfaces.

should be considered as excited states since they are above the ground state. Calculation of vibrational frequencies associated to all states confirm that stable structures correspond to minima of the electronic energy surface. DPA2, DPA4 and DPA6 have C_{2v} symmetry while the other three isomers are C_s. Electronic state energies (E), binding energies (BE), dipole moments, ionization potentials (IP), adiabatic electronic affinities (EA), and HOMO–LUMO gaps (Δ) for the six predicted isomers are summarized in Table 1. The binding energy is defined as BE = $|E_{DPA} - E_{atomic}|$, where E_{atomic} is the sum of the individual atom energies. The IP and EA are

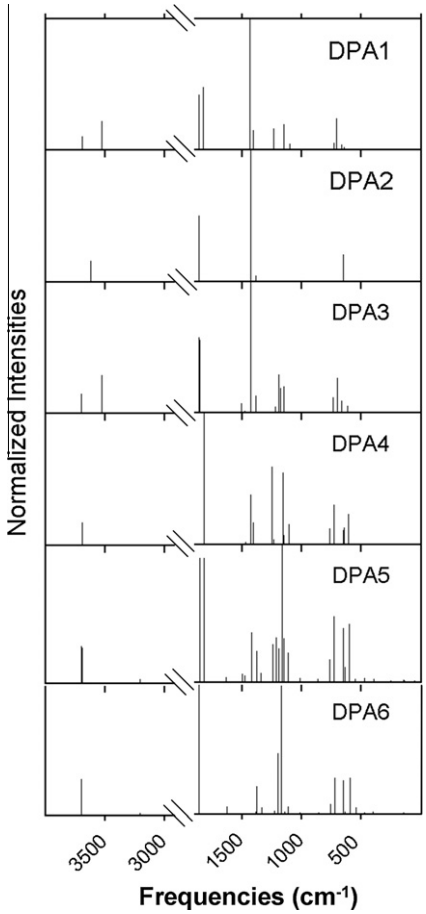

Fig. 3. Calculated infrared spectra of the six gas phase isomers of DPA.

calculated as differences between the optimized state of the neutral and the optimized state of the cation or anion, respectively. The zero point energies (ϵ) of the six isomers is very similar, about 3.2 eV.

DPA1 is the global minimum structure taking into account that its total electronic energy plus the zero point energy is the lowest of the six predicted structures. Two isomers, DPA2 and DPA3, lie in almost degenerate states above the DPA1 structure at 0.046 and 0.050 eV, respectively. Isomers DPA4, DPA5, and DPA6 lie higher up above DPA1 at 0.144, 0.215, and 0.296 eV, respectively. The DPA6 isomer has previously been proposed by Carmona [16] as the unique structure for DPA. The DPA5 isomer is the structure proposed in Ref. [30] and determined by Tellez et al. [17] to be the main component in DPA supramolecular arrays. The structure of the DPA4 isomer was reported in previous calculations [21] and identified experimentally in Raman measurements [31]. It is thus important to point out that three additional stable isomers, put forward in this paper, are new to the literature. The ionization potential of the three most stable isomers is larger than the reminding three. Additionally, DPA1, DPA2, and DPA3 have significantly larger electron affinities, making them more reactive than the others. The HOMO–LUMO gap is quite large in all six isomers. The spectrum of one-electron Khon-Sham molecular orbital levels for the monomeric isomers is given in the Supplementary data. It is interesting to note that the more symmetric monomers show degeneracies in the valence and virtual states that disappear in the less symmetric isomers. Of all isomers, DPA3 is the most polar compound out of the six studied structures.

A Mulliken analysis of the wave function yields charges on the different atoms which are very similar across the six isomers as

Table 3
Calculated vibrational spectrum of the DPA isomer with lowest energy and comparison with experiments.

DPA1			Experiment[16]	
ν (cm^{-1})	Intensity	Assignment	IR	Raman
3692	81	υ OH	3115	3113
3530	145	υ OH	3102	3105
3246	0	υ_s C–H		3070
3243	1	υ_a C–H	3070	
3212	7	υ_a C–H	2800	2650
1863	253	υ C=O	1710	1646
1825	287	υ C=O	1700	1640
1644	2	υ ring C–C	1576	1580
1630	3	υ ring C–C, C–N	1571	1577
1508	7	ρ CH	1470	1475
1469	15	υ C–N	1468	1447
1437	572	σ OH	1422	1439
1405	108	σ OH	1387	1423
1355	16	υ ring C–C, C–N	1341	1332
1277	14	σ OH, υ C–C	1308	1304
1236	114	σ OH	1275	1279
1185	8	σ CH	1260	1262
1165	10	υ C–O	1178	1183
1152	132	υ C–O	1151	1156
1102	50	σ CH	1082	1090
1028	0	ω CH	998	
1023	10	ring breath	987	998
974	0	ω CH	937	987
898	11	υ C–C, ρ ring	890	895
862	13	ω CH	855	855
796	22	τ full molecule	751	802
767	5	ω CH	705	762
742	2	ring breath, σ C (=O)–O	692	752
731	55	ω OH	668	698
709	156	ω C–C/O–H	647	647
663	48	ρ in-plane	592	630
645	37	ring breath	583	619
625	32	ω OH	530	
576	3	ρ in-plane	519	495
478	2	ρ in-plane	421	491
467	11	ω ring	365	437
437	0	ρ out-of-plane	330	396
384	4	ρ in-plane	226	298
359	2	ring breath	218	209
259	20	ρ in-plane	208	192
176	2	τ ring	199	135
155	1	ρ out-of-plane	107	121
131	5	σ full molecule	89	85
82	4	τ C-COOH	79	72
55	3	τ C-COOH		28

υ, stretching; ω, wagging; ρ, rocking; τ, twisting; σ, scissoring; Ph, phenyl. Subscripts: *a*, asymmetric; *s*, symmetric.

shown in Table 2. The Fukui function [32] $f(\mathbf{r})=\partial\rho(\mathbf{r})/\partial N$ is evaluated from right or left to avoid the discontinuity at integer N yielding the electron acceptor function f^+ (derivative taken from the right)

$$f^+(\mathbf{r}) = \rho_{N+1}(\mathbf{r}) - \rho_N(\mathbf{r}) \quad (1)$$

and the electron donor function f^- (derivative taken from the left)

$$f^-(\mathbf{r}) = \rho_N(\mathbf{r}) - \rho_{N-1}(\mathbf{r}) \quad (2)$$

where $\rho_N(\mathbf{r})$ is the electron density of a system with N electrons [33]. These functions are useful for predicting the nucleophilic and electrophilic reactivity of compounds. The reactivity indicator for radical attack is defined by

$$f^0(\mathbf{r}) = \frac{1}{2}(f^+(\mathbf{r}) + f^-(\mathbf{r})) \quad (3)$$

The Fukui functions f^- and f^0 for DPA are shown in Fig. 2. The calcium salt of DPA involves electrophilic substitution with a calcium dication displacing two hydrogens to form CaDPA. Thus, DPA is an electron donor molecule. We see in Fig. 2 that DPA4 has the largest

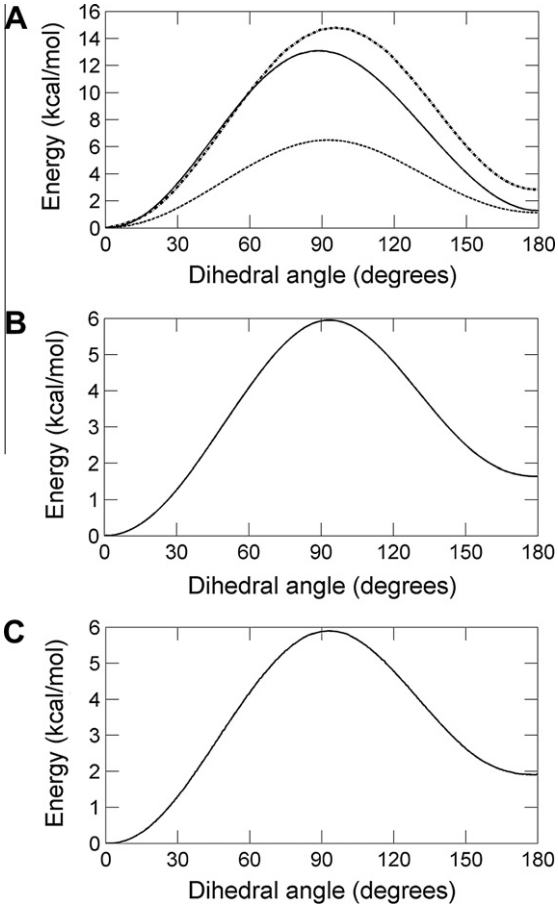

Fig. 4. Energy pathways for five different reactions: (a) DPA1 to DPA2 [solid], DPA1 to DPA3 [small dots], DPA1 to DPA4 [large dots], (b) DPA4 to DPA5, (c) DPA5 to DPA6. The energies in (a–c) are relative to the DPA1, DPA4, and DPA5 minima, respectively.

f^- value at the nitrogen site. The other isomers have similarly large f^- values at the nitrogen site except for DPA2. All of the isomers show a large f^- value at the carboxyl oxygens (8 and 11 in Fig. 1). The binding site for a calcium atom to DPA is likely to occur near the nitrogen or carboxylic oxygens.

Inspection of the f^0 Fukui function shows that it is similar to f^-. Sites susceptible to radical attack are the nitrogen atom and carboxyl oxygens for DPA1, DPA2, and DPA6 while DPA3 only has high f^0 at the carboxyl oxygen #11 site. DPA4 has high f^0 only at the nitrogen and DPA5 has high f^0 at the nitrogen and moderately high f^0 at the oxygen #11 site.

The calculated vibrational spectra of all six monomers are shown in Fig. 3, where peak heights are normalized to the peak of maximum intensity for each isomer. Assignment of the normal modes of vibration in DPA1 is given in Table 3 and compared with experiment [16]. Frequencies for the other five isomers are reported in the Supplementary data. It is interesting to note that DPA1 through DPA3 have similar spectra, and these are quite different than the spectra of the other three isomers. All isomers have prominent OH stretching modes in the high frequency range (>3500 cm^{-1}). The two OH stretching modes for DPA1 (3692 and 3530 cm^{-1}) and DPA3 (3699 and 3524 cm^{-1}) are clearly split while the other isomers' OH stretching modes are almost exactly overlapping. The OH stretching modes of DPA4, DPA5, and DPA6 are also blue-shifted from those of DPA1, 2, and 3. The quite intense C=O stretching mode is seen in all of the monomers between 1816 and 1868 cm^{-1}. A slight splitting of the C=O stretching modes

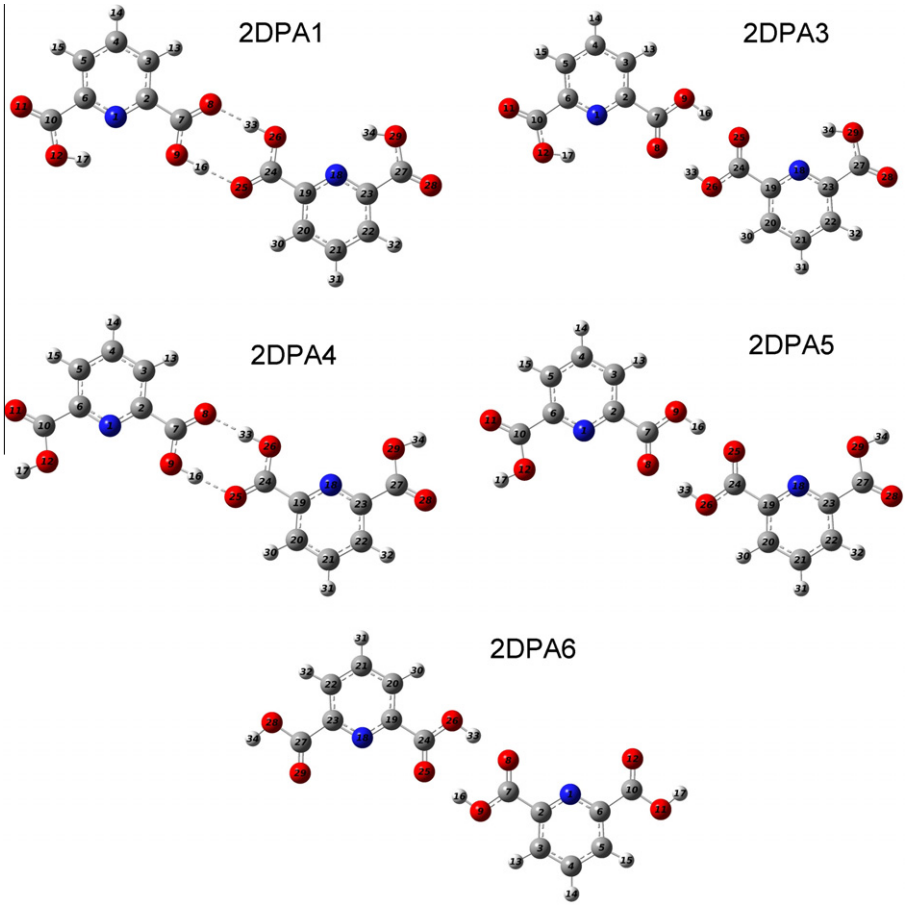

Fig. 5. Structure of optimized dimers of DPA showing the tandem of hydrogen bonds required for forming them.

Table 4
Electronic states, total electronic energies, zero point energies (ϵ_0), dimer formation energies ($E_{formation}$), electron affinities (EA), ionization potentials (IP), and HOMO–LUMO gap (Δ) of DPA dimers. Total electronic energies E are relative to the 2DPA1 ground state energy of −34.038310 keV.

Dimer	State	E (eV)	ϵ_0 (eV)	$E_{formation}$ (eV)	EA (eV)	IP (eV)	Δ (eV)
2DPA1	$^1A_1$	0	6.514	0.818	1.264	8.928	5.089
2DPA3	$^1A_1$	0.042	6.510	0.875	1.255	8.917	5.084
2DPA4	$^1A_1$	0.292	6.498	0.814	0.813	8.553	5.353
2DPA5	$^1A_1$	0.351	6.492	0.898	0.804	8.580	5.388
2DPA6	$^1A_1$	0.501	6.482	0.908	0.775	8.695	5.551

in DPA1 and DPA5 is also noticeable. The 1863 cm^{-1} line in DPA1 is due to the C10–O11 stretching mode and the 1825 cm^{-1} line is due to the C7–O8 stretching mode. Meanwhile in DPA5, the 1855 cm^{-1} line is due to the C7–O8 stretching mode and the 1818 cm^{-1} line is due to the C10–O11 stretching mode.

The most intense mode in DPA1, DPA2, and DPA3 is the OH scissoring mode located at 1400 and 1440 cm^{-1}. In all three of these modes, H17 is swung towards the nitrogen. For the DPA2 OH scissoring mode, both H16 and H17 have the same swinging motion inwards to N1. Those same OH scissoring modes exist for DPA4, DPA5, and DPA6 but their motion brings the hydrogen closer to the carboxyl oxygen and results in a lower intensity line. The DPA4, DPA5, and DPA6 C–O stretching and CH scissoring modes between 1100 and 1170 cm^{-1} are very intense. These same modes are present in DPA1, DPA2, and DPA3 but are less intense. The most prominent feature for DPA1, DPA2, and DPA3 below 1000 cm^{-1} is the C–C and OH wagging mode. This mode appears at approximately 700 cm^{-1}. Meanwhile, for DPA4, DPA5, and DPA6, several moderately intense lines lie between 600 and 800 cm^{-1}. These lines are due to the OH wagging mode (590–615 cm^{-1}), the in-plane rocking mode (645–655 cm^{-1}), the out-of-plane rocking mode (700–735 cm^{-1}), and the CH wagging mode (750–770 cm^{-1}). The only moderately intense lines for DPA1, DPA2, and DPA3 below 1000 cm^{-1} belong to the C–C and OH wagging modes between 670 and 740 cm^{-1}.

The rotational constants of all six isomers are quite similar. These rotational constants in GHz are 1.76967, 0.64388, and 0.47210 for DPA1, 1.77310, 0.64430, 0.47258 for DPA2, 1.80582, 0.63269, 0.46853 for DPA3, 1.79468, 0.62793, 0.46517 for DPA4, 1.83484, 0.61616, 0.46126 for DPA5, and 1.87671, 0.60428, 0.45710 for DPA6.

Several isomerization reaction coordinates are predicted and the transition state in each reaction is identified using the synchronous transit-guided quasi-Newton method [34,35]. The energy paths for the five isomerization reactions are shown in Fig. 4. Reaction pathways are calculated along the intrinsic reaction coordinates (IRC). The structure of the compound at the transition state is confirmed through vibrational analysis by displaying one imaginary frequency. All of the transition structures are near the midpoint (±90°) geometry of complete dihedral angle rotations: DPA1 → DPA2 (2,7,9,16) dihedral; DPA1 → DPA3 (1,2,7,8) dihedral, DPA1 → DPA4 (6,10,12,17) dihedral; DPA4 → DPA5 (1,2,7,8) dihedral; and DPA5 → DPA6 (5,6,10,11) dihedral. Thus; the IRC transition vectors chosen are the dihedral angles differentiating the two isomers. As seen in Fig. 4, the barriers for these rearrangement reactions are between 6 and 14 kcal/mol, not

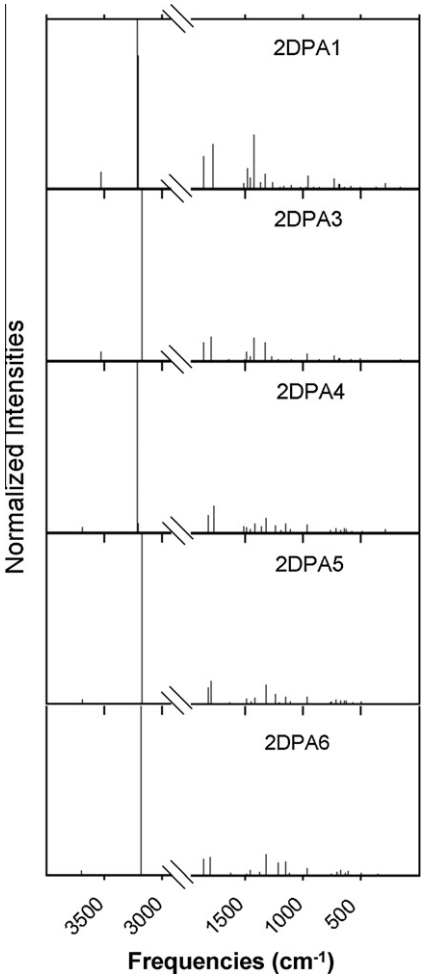

Fig. 6. Calculated infrared spectra of the five dimers of DPA in the gas phase.

attainable at room temperature from either side of the reaction path. The most favorable rearrangement is DPA1 into DPA3 (Fig. 4A small dots line) which carries a cost of about 6 kcal/mol. The rearrangement reaction of DPA1 into DPA2 or DPA4 requires twice as much energy (13.1 and 14.8 kcal/mol, respectively) as shown in Fig. 4A. It is interesting to note that the isomerization reaction from DPA4 to DPA5 (Fig. 4B) and DPA5 to DPA6 (Fig. 4C) are possible when a barrier of 6 kcal/mol is surmounted.

In summary, based on the isomerization energy barriers obtained, DPA1 (most stable isomer) is unlike to isomerize at normal laboratory conditions to any of the other five stable isomers. In addition, assuming that under certain thermodynamic conditions one of the less stable isomers is formed, this isomer would quite unlikely rearrange into any of the other five (the energy barriers are too high). For this reason, in the following section we study dimerization reactions that involve only one type of isomer in each case. When compared to isomerization of other rotamers such as methyl salicylate ketoB → ketoA, barriers of 6 kcal/mol are lower by a factor of three [36]. However, dihedral angle isomerization barriers from anti-gauche → syn-gauche in bipyrrole are five times smaller [37].

3. DPA dimers

There are a number of planar aromatic molecules that dimerize by means of two in-plane inter-monomer hydrogen bonds that contribute to their stabilization. An example is the benzoic acid dimer [38] that further enters as a molecular entity in the crystal [39]. However, benzoic acid dimers do not allow for chain-like supramolecular structures linked by double intermolecular hydrogen bonds. A number of DPA dimers are plausible to be predicted when two molecules bind by means of two hydrogen bonds and remain planar. We study here several possibilities within the same DFT level of calculation. The purpose of this search is to find dimers with two intermolecular hydrogen bonds that would be prone to further form trimers, and larger arrays if more DPA monomers are added. The search was restricted to isomers of the same kind. This is because the chemical equilibrium between isomers of different types involve conditions away from normal temperature and pressure, as has been discussed in the previous section. Five stable and optimized dimer structures are shown in Fig. 5. All structures have C_{2h} symmetry. The notation adopted for identifying these dimers is 2DPAn, $n = 1, 3–6$. These dimers of two DPA molecules bind through two inter-molecular hydrogen bonds (O–H–O) joining the COOH groups. Dimers of DPA2 are absent because there is no possible O–H–O bonds between two DPA2 monomers. The electronic states, energies, zero point energy, formation energies, ionization potential, electronic affinity, and HOMO–LUMO gap for these five dimers are reported in Table 4. The DPA1 dimer (2DPA1) is the lowest in energy of the five dimers investigated. In Table 4, the energy of each dimer is referred to the energy of the 2DPA1. As for the monomers, the zero point energies are very comparable for the five isomers. The formation energy $E_{formation} = 2E_{monomer} - E_{dimer}$ is lowest for 2DPA4, which also has the lowest IP. For a balance of energies, 2DPA4 is then quite effective for forming supramolecular structures such as chains linked through pairs of O–H–O bonds. Additionally, this isomer is the central unit for forming the crystal. We note that despite the fact that 2DPA1 is the lowest in energy, this dimer and 2DPA3 may only exist in the gas or liquid phases since there are no paths for forming inter-molecular hydrogen bonds. Electron affinities and HOMO–LUMO gap, are quite comparable for the five dimers. Also notable is the expected shrinkage of the HOMO–LUMO gap in the dimers when compared to gaps in the monomers (Table 1). It is possible to mix and match different DPA isomers to form other dimers but such speculation is not part of this work.

All five DPA dimers are non-polar with zero dipole moments. Calculation of the vibrational frequencies confirms that the structures reported in Fig. 5 are minima. The calculated vibrational IR spectra for the DPA dimers are shown in Fig. 6. The OH stretching mode at frequencies 3100 and 3200 cm^{-1} is quite dominant and overshadows the spectrum in all five dimers. It has been pointed out [31,40] that the O–H vibrational stretching bands are blue shifted as DPA changes phase from vapor → liquid → solid. A blue shift of the O–H stretching modes from 400 to 500 cm^{-1} is already present when comparing the monomer to the dimer spectra.

Various out-of-plane dimers were attempted. However, in the few cases that stable structures were found, these were at least 0.6 eV higher in energy than the planar dimers. By stacking two 2DAP4 dimers and optimizing the geometry of the supramolecular arrangement, we find that the two dimers tend to form a fan-looking structure in which the initially parallel planes organize themselves at a 45° angle.

4. DPA crystalline polytypes

Several of the DPA dimer structures lend themselves to be extended in linear chains by adding more monomers. Using the same DFT level of calculation plus periodic boundary conditions (PBC), one-dimensional chains of DPA4, DPA5, and DPA6 are optimized and found to be stable. The initial guess of 16.167 Å for the lattice parameter (i.e., two monomers long) was taken from experimental

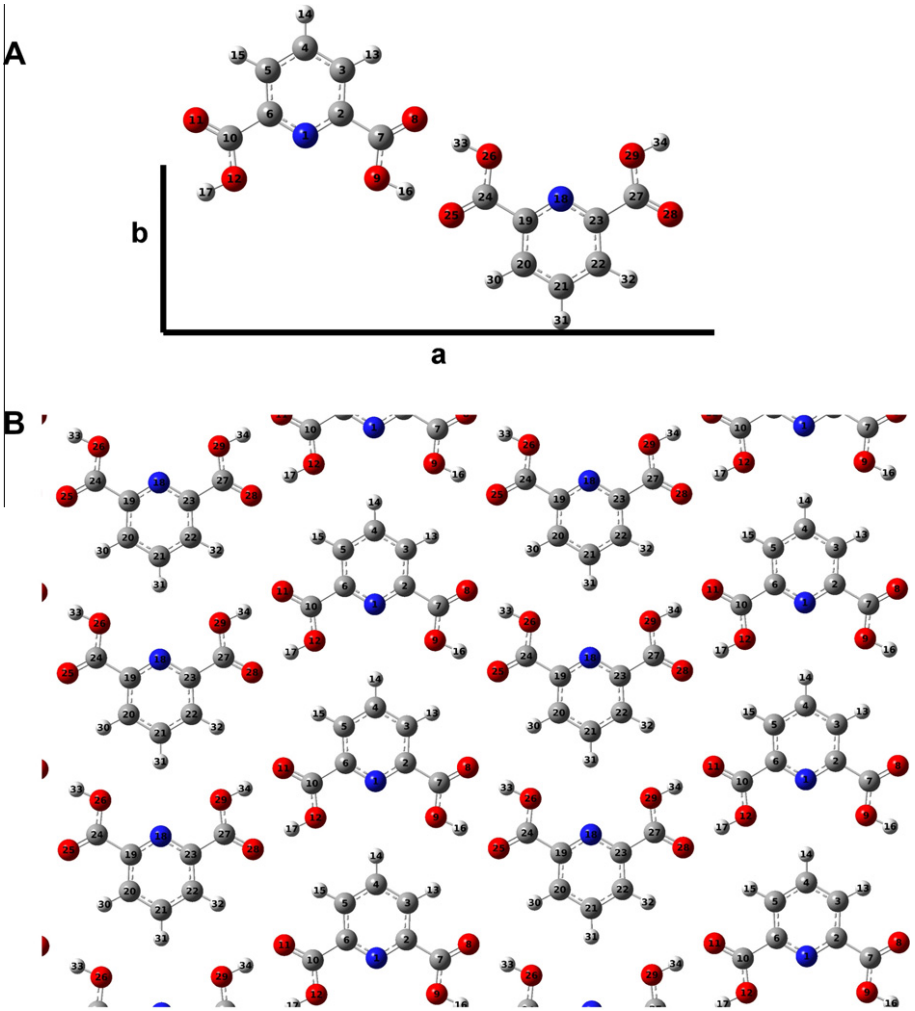

Fig. 7. Sheet formation of DPA4 in two dimensions showing the arrangement of parallel chains in the plane. (a) Optimized unit cell with lattice constants of a = 16.398 Å and b = 6.754 Å; (b) a 2 × 2 supercell.

crystallographic data [17] of DPA crystals. The chain of DPA4 has the lowest total energy of the three. The DPA5 and DPA6 chains have energies of 0.060 and 0.156 eV above the DPA4 chain, respectively. The optimized lattice parameters have lengths of 16.497, 16.318, and 16.257 Å for DPA4, DPA5, and DPA6 chains, respectively. These values are slightly expanded (at most 2%) with respect to the experimental observation in the crystal.

These optimized 1-D chains and X-direction translation vectors are then used as the initial guesses for a two-dimensional calculation of DPA4, DPA5, and DPA6. The initial guess for the lattice constant in the y-direction is 5.571 Å, again taken from experiments [17] of crystalline DPA. The energies of the optimized sheets are nearly degenerate with the 2DPA4 sheet having the lowest total energy. The DPA5 and DPA6 sheets have total energies of 0.022 and 0.041 eV above that of the DPA4 sheet, respectively. The 2-D optimization results agree with the crystal structure of previous experiments [17] and show that chains of DPA arrange themselves in rows within a plane as illustrated in Fig. 7. However, the calculation predicts larger unit cell lengths along the XY-plane than experiment. The optimized lattice constants are (16.398,6.754), (16.376,6.690), and (16.378,6.611) Å for the DPA4, DPA5, and DPA6 2-D sheets, respectively. Finally, single point calculation of three-dimensional crystal structures of DPA4, DPA5, and DPA6 are calculated by stacking the optimized 2-D sheets on top of each other with an inter-plane distance c = 3.77 Å. The c lattice constant is again taken from experiments [17]. The energy ordering of the three structures is nearly identical to the 2-D case, with DPA5 and DPA6 crystal structures having total energies of 0.022 and 0.042 eV above that of the DPA4 crystal, respectively.

These DPA layered crystals are orthorhombic. The band structures of the three crystalline forms are then plotted along characteristic symmetry lines of the irreducible Brillouin zone [41] and shown in Fig. 8 for the DPA4 crystal. Nine occupied and nine unoccupied bands are plotted along the edges and two faces of one eighth of the irreducible Brillouin zone. All energies in Fig. 8 are referred to the Fermi energy level of the DPA crystal, which is computed by solving self-consistently the expression equating the number of electrons (N) to the sum of electron occupation probabilities (Fermi functions) of states composing the bands [42],

$$N = \sum_{\alpha=1}^{n_{band}} \sum_{k=1}^{n_k} \frac{2}{1 + e^{\frac{E_{\alpha,k} - E_F}{k_B T}}} \tag{4}$$

where n_{band} = 20 is the number of bands, n_k = 144 is the number of k-points in each band, k_B is Boltzmann's constant, and T = 300 K. Accuracies better than 0.001 eV were achieved in the determination of E_F. The calculated Fermi energy of the DPA4 crystal is −7.534 eV. As expected, this crystal is an insulator with indirect band gap of 4.84 eV and direct band gap of 5.02 eV. The DPA5 crystal has a Fermi energy of −7.679 eV, indirect band gap of 4.85 eV and direct band

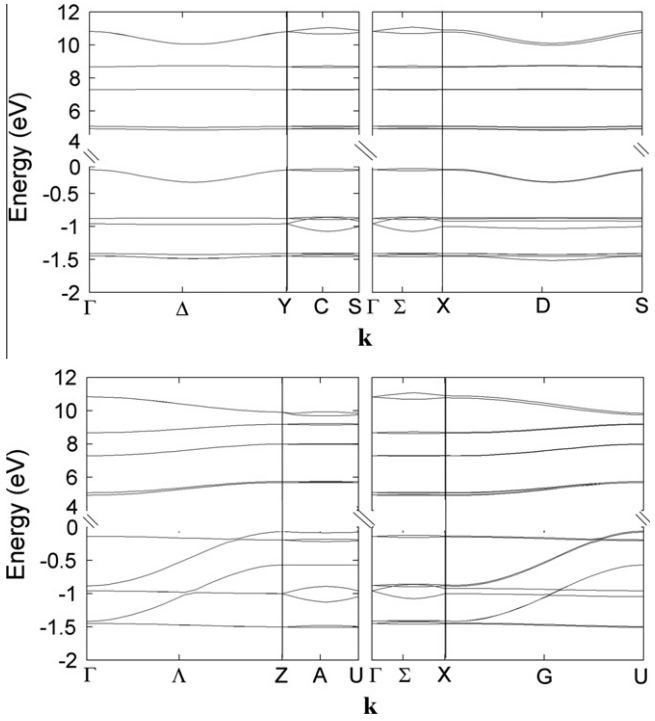

Fig. 8. Band structure of the orthorhombic DPA4 crystal calculated along symmetry lines Δ, C, Σ, D (top) and symmetry lines Λ, A, Σ, G (bottom).

gap of 5.08 eV. The Fermi energy of the DPA6 crystal is −7.770 eV and has an indirect band gap of 4.85 eV and a direct band gap of 5.15 eV.

5. Conclusion

The structure, energetics, and vibrational analyses of six gas phase isomers and dimers of neutral, anhydrous, DPA have been calculated within the DFT B3LYP/6-31G (d) computational modeling frame. All structures were determined to be stable in singlet ground states and triplet excited states. In the gas phase we predict that DPA1 is the most abundant isomer. Populations of DPA2 and DPA3 may also exist in the gas phase as those two isomers have almost degenerate ground states at ≈0.05 eV above the DPA1 structure. Ionization potentials of all these isomers are high (above 9 eV) and the HOMO–LUMO energy gap is substantial of about 5 eV. Transition states between five possible isomeric reactions were found plausible at high temperatures, demonstrating that the DPA1 → DPA3 and DPA4 → DPA5 reactions are energetically most favorable with a barriers of about 6 kcal/mol. The least favorable isomerization reaction is DPA1 →;DPA4 with a barrier of 14.8 kcal/mol. Experiments of DPA in the gas phase are long overdue, and we expect that our predictions may lead to future experiments.

Clear differences exist between the vibrational spectra of the crystal-forming monomers of DPA (4, 5, and 6) and the lower energy monomers (1, 2, and 3) which we theorize to only exist in vapor and liquid phases. The most evident difference is the much larger IR intensity of the O–H scissoring modes at 1420 and 1440 cm^{-1} for the 1, 2, and 3 isomers. Another important difference appears for the C–H scissoring modes at 1160 and 1200 cm^{-1} which are more intense for the crystal-forming monomers than for the 1, 2, and 3 forms. We predict that only DPA4, DPA5, and DPA6 can aggregate in supramolecular linear chains. When these chains are laid parallel lengthwise on a plane, we have demonstrated that planar sheets are stable, well bound 2-D structures.

The crystal forming DPA4, DPA5, and DPA6 originate three crystal polytypes, all three being lattices formed by stacking DPA sheets. These three crystals are basically degenerate in energy. Their orthorhombic crystal structure is quite similar and all three polytypes are insulators. DPA5 and DPA6 crystals have been mentioned in the literature [17,16]. The three now confirmed crystal structures of DPA4, DPA5, and DPA6 deserve future experimental study. During the first step of germination, spore-specific DPA is released [43]. Speculating that different markers may be devised with these three crystalline polytypes, our predictions may help with tailoring DPA for measuring the specificity of germinated spores. The three neutral isomers DPA1, DPA2, DPA3, now confirmed to be stable structures, may be source of alternative zwitterion structures displaying hypochromism or hyperchromism [19] since their electron affinity is three times larger than the electron affinity of the crystal-forming isomers.

Acknowledgement

This work was partially supported under the National Science Foundation Grant CHE-0626111. We acknowledge the Teragrid allocation award CHE100033 and the USACE ERDC MSRC for the extensive software and computational resources.

Appendix A. Supplementary material

Supplementary data associated with this article can be found, in the online version, at doi:10.1016/j.comptc.2011.09.030.

References

[1] J.F. Powell, R.E. Strange, Biochemical changes occurring during the germination of bacterial spores, Biochem. J. 54 (1953) 205–209.
[2] J.F. Powell, Isolation of dipicolinic acid from spores of bacillus megatherium, Biochem. J. 54 (1953) 210–211.
[3] M.L. Cable, J.P. Kirby, K. Sorasaenee, H.B. Gray, A. Ponce, Bacterial spore detection by [Tb^{3+}(macrocycle)(dipicolinate)] luminescence, J. Am. Chem. Soc. 129 (2007) 1474–1475.
[4] T.A. Slieman, W.L. Nicholson, Role of dipicolinic acid in survival of bacillus subtilis spores exposed to artificial and solar UV radiation, Appl. Environ. Microbiol. 67 (2001) 1274–1279.
[5] C. Desnous, D. Guillaume, P. Clivio, Spore photoproduct: a key to bacterial eternal life, Chem. Rev. 110 (2010) 1213–1232.
[6] S. Matys, J. Ra, U. Soltmann, S. Selenska-Pobell, H. Böttcher, W. Pompe, Calcium dipicolinate induced germination of bacillus spores embedded in thin silica layers: novel perspectives for the usage of biocers, Chem. Mater. 16 (2004) 5549–5551.
[7] P. Zuber, Management of oxidative stress in bacillus, Ann. Rev. Microbiol. 63 (2009) 575–597.
[8] D.L. Rosen, C. Sharpless, L.B. McGown, Bacterial spore detection and determination by use of terbium dipicolinate photoluminescence, Anal. Chem. 69 (1997) 1082–1085.
[9] P.M. Pellegrino Jr., N.F. Fell, D.L. Rosen, J.B. Gillespie, Bacterial endospore detection using terbium dipicolinate photoluminescence in the presence of chemical and biological materials, Anal. Chem. 70 (1998) 1755–1760.
[10] A.A. Hindle, E.A.H. Hall, Dipicolinic acid (DPA) assay revisited and appraised for spore detection, Analyst 124 (1999) 1599–1604.
[11] T.K. Prasad, M.V. Rajasekharan, $[M(dipicH_2)(H_2O)_3]^{2+}$ M = Ni, Cu, Zn ($dipicH_2$= dipicolinic acid): a combined crystallographic, spectroscopic and computational study, Polyhedron 26 (2007) 1364–1372.
[12] J. Anderson, J. Nelson, C. Reynolds, D. Ringelberg, G. Tepper, D. Pestov, Steady-state and frequency-domain lifetime measurements of an activated molecular imprinted polymer imprinted to dipicolinic acid, J. Fluoresc. 14 (2005) 269–274.
[13] P.D. Kwong, R. Wyatt, J. Robinson, R.W. Sweet, J. Sodroski, W.A. Hendrickson, Structure of an HIV gp120 envelope glycoprotein in complex with the CD4 receptor and a neutralizing human antibody, Nature 393 (1998) 648–659.
[14] S. Sarasndarajah, J. Kunnil, B.V. Bronk, L. Reinisch, Two dimensional multiwavelength fluorescence spectra of dipicolinic acid and calcium dipicolinate, Appl. Opt. 44 (2005) 1182–1187.
[15] R. Nudelman, B.V. Bronk, S. Efrima, Fluorescence emission derived from dipicolinic acid, its sodium, and its calcium salts, Appl. Spectrosc. 54 (2000) 445–449.
[16] P. Carmona, Vibrational spectra and structure of crystalline dipicolinic acid and calcium dipicolinate trihydrate, Spectrochim. Acta, Part A 36 (1980) 705–712.

[17] V.C. Téllez, B.S. Gaytán, S. Bernés, E.G. Vergara, The supramolecular structure of pyridine-2,6-dicarboxylic acid, Acta. Cryst. C58 (2002) 228–230.
[18] M.C. Grossel, A.N. Dwyer, M.B. Hursthouse, J.B. Orton, Polymorphism in pyridine-2,6-dicarboxylic acid: competition between robust synthons, Cryst. Eng. Commun. 8 (2006) 123–128.
[19] F. Peral, E. Gallego, Self-association of pyridine-2,6-dicarboxylic acid in aqueous solution as determined from ultraviolet hypochromic and hyperchromic effects, Spectrochim. Acta, Part A 56 (2000) 2149–2155.
[20] K.E. Edgecombe, D.F. Weaver, V.H. Smith Jr., Electronic structure lysis of compounds of interest in drug design: mono- and dicarboxylated pyridines, Can. J. Chem. 72 (1994) 1388–1403.
[21] H.F. Hameka, J.O. Jensen, L.J. Jensen, C.N. Merrow, C.P. Vlahacos, Theoretical studies of the fluorescence of dipicolinic acid and its anion, J. Mol. Struct. (Theochem.) 365 (1996) 131–141.
[22] J.R. Xie, V.H. Smith Jr., R.E. Allen, Spectroscopic properties of dipicolinic acid and its dianion, Chem. Phys. 322 (2006) 254–268.
[23] A. Picot, C. Feuvrie, C. Barsu, F. Malvolti, B. Le Guennic, H. Le Bozec, C. Andraud, L. Toupet, O. Maury, Synthesis, structures, optical properties, and TD-DFT studies of donor-π-conjugated dipicolinic acid/ester/amide ligands, Tetrahedron 64 (2008) 399–411.
[24] B.S. Parajón-Costa, O.E. Piro, R. Pis-Diez, E.E. Castellano, A.C. Gonzalez-Baro, Crystal structures, spectroscopic characterization and theoretical calculations of the guanidinium and ammonium salts of the insulin-enhancing anion $[VO_2(dipic)]^-$, Polyhedron 25 (2006) 2920–2928.
[25] A. DAleo, A. Picot, A. Beeby, J.A.G. Williams, B. Le Guennic, C. Andraud, O. Maury, Efficient sensitization of europium, ytterbium, and neodymium functionalized tris-dipicolinate lanthanide complexes through tunable charge-transfer excited states, Inorg. Chem. 47 (2008) 10258–10268.
[26] C. Gonzalez-Baro, R. Pis-Diez, O.E. Piro, B.S. Parajón-Costa, Crystal structures, theoretical calculations, spectroscopic and electrochemical properties of Cr(III) complexes with dipicolinic acid and 1,10-phenantroline, Polyhedron 27 (2008) 502–512.
[27] C. Lee, W. Yang, R.G. Parr, Development of the Colle-Salvetti correlation-energy formula into a functional of the electron density, Phys. Rev. B 37 (1988) 785–789.
[28] X. Li, M.J. Frisch, Energy-represented DIIS within a hybrid geometry optimization method, J. Chem. Theory Comput. 2 (2006) 835–839.
[29] M.J. Frisch, G.W. Trucks, H.B. Schlegel, G.E. Scuseria, M.A. Robb, J.R. Cheeseman, G. Scalmani, V. Barone, B. Mennucci, G.A. Petersson, H. Nakatsuji, M. Caricato, X. Li, H.P. Hratchian, A.F. Izmaylov, J. Bloino, G. Zheng, J.L. Sonnenberg, M. Hada, M. Ehara, K. Toyota, R. Fukuda, J. Hasegawa, M. Ishida, T. Nakajima, Y. Honda, O. Kitao, H. Nakai, T. Vreven, J.A. Montgomery, Jr., J.E. Peralta, F. Ogliaro, M. Bearpark, J.J. Heyd, E. Brothers, K.N. Kudin, V.N. Staroverov, R. Kobayashi, J. Normand, K. Raghavachari, A. Rendell, J.C. Burant, S.S. Iyengar, J. Tomasi, M. Cossi, N. Rega, J.M. Millam, M. Klene, J.E. Knox, J.B. Cross, V. Bakken, C. Adamo, J. Jaramillo, R. Gomperts, R.E. Stratmann, O. Yazyev, A.J. Austin, R. Cammi, C. Pomelli, J.W. Ochterski, R.L. Martin, K. Morokuma, V.G. Zakrzewski, G.A. Voth, P. Salvador, J.J. Dannenberg, S. Dapprich, A.D. Daniels,. Farkas, J.B. Foresman, J.V. Ortiz, J. Cioslowski, D.J. Fox, Gaussian 09 Revision A.1., 2009, Gaussian Inc., Walli.
[30] F. Takusagawa, K. Hirotsu, A. Shimada, The crystal structure of dipicolinic acid monohydrate, Bull. Chem. Soc. Jpn. 46 (1973) 2020–2027.
[31] A.A. Kolomenskii, H.A. Schuessler, Raman spectra of dipicolinic acid in crystalline and liquid environments, Spectrochim. Acta, Part A 61 (2005) 647–651.
[32] P.W. Ayers, W. Yang, L.J. Bartolotti, Fukui function, in: Chemical Reactivity Theory: A Density Functional View, CRC Press, Boca Raton, 2009, pp. 255–267 (Chapter 18).
[33] K. Fukui, Role of frontier orbitals in chemical reactions, Science 217 (1982) 747–784.
[34] C. Peng, P.Y. Ayala, H.B. Schlegel, M.J. Frisch, Using redundant internal coordinates to optimize equilibrium geometries and transition states, J. Comput. Chem. 49 (1996) 49–56.
[35] C. Peng, H.B. Schlegel, Combining synchronous transit and quasi-newton methods to find transition states, Isr. J. Chem. 33 (1993) 449–454.
[36] R.D. Massaro, Y. Dai, E. Blaisten-Barojas, Energetics and vibrational analysis of methyl salicylate isomers, J. Phys. Chem. A 113 (2009) 10385–10390.
[37] Y. Dai, E. Blaisten-Barojas, Energetics, structure, and charge distribution of reduced and oxidized n-pyrrole oligomers: a density functional approach, J. Chem. Phys. 129 (2008) 164903.
[38] M.J. Wójcik, K. Szczeponek, M. Boczar, Theoretical study of multidimensional proton tunnelling in benzoic acid dimer, Int. J. Mol. Sci. 4 (2003) 422–433.
[39] M.R. Johnson, H.P. Trommsdor, Dispersion of vibrational modes in benzoic acid crystal, Chem. Phys. Lett. 364 (2002) 34–38.
[40] F.R. Dollish, W.G. Fateley, F.F. Bentley, Characteristic Raman Frequencies of Organic Compounds, Wiley, New York, 1974.
[41] T. Grandke, L. Ley, Angular-resolved uv photoemission and the band structure of GeS, Phys. Rev. B 16 (1977) 832–842.
[42] Y. Dai, S. Chowdhury, E. Blaisten-Barojas, Density functional theory study of the structure and energetics of negatively charged oligopyrroles, Int. J. Quantum Chem. 111 (2011) 2295–2305.
[43] P. Setlow, Spore germination, Curr. Opin. Microbiol. 6 (2003) 550–556.